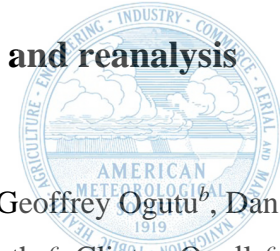# The Turkana Jet diurnal cycle in observations and reanalysis

Callum Munday,[a] Sebastian Engelstaedter,[a] Richard Washington,[a] Geoffrey Ogutu[b], Dan Olago[c], Gilbert Ouma[c], James Warner[d], Dennis Ong'ech[c], Rose Nkatha[c], Clinton Ogolla[c], Bonface Wanguba[c]

[a] *Climate Research Lab, School of Geography and the Environment, University of Oxford, Oxford, United Kingdom*

[b] *Kenya Meteorology Department, Nairobi, Kenya*

[c] *Institute for Climate Change and Adaptation, University of Nairobi, Nairobi, Kenya*

[d] *Met Office, Exeter, United Kingdom*

Corresponding author: Callum Munday, callum.munday@ouce.ox.ac.uk

1

ABSTRACT

The Turkana Jet is an equatorial low-level jet (LLJ) in East Africa. The jet influences both flooding and droughts, and powers Africa's largest wind farm. Much of what we know about the jet, including the characteristics of its diurnal cycle, derives from reanalysis simulations which are not constrained by radiosonde observations in the region. Here, we report the characteristics of the Turkana Jet with data from a field campaign during March-April 2021 - The Radiosonde Investigation For the Turkana Jet (RIFTJet). The southeasterly jet forms on average at 380 m above the surface, with mean speeds of 15.0 m.s^{-1}. The strongest low-level winds are during the night and early morning from 0300 LT to 0600 LT (>16 m.s^{-1}). The average wind profile retains a characteristic low-level jet structure throughout the day, with the low-level wind maximum weakening to a minimum of 10.9 m.s^{-1} at 1500 LT. There is significant shear, of up to 1.5 m.s^{-1} per 100 m maintained through the 1000 m above the wind maximum. The diurnal cycle of the jet is associated with the nocturnal strengthening and lowering of elevated subsidence inversions, which form above the jet. Reanalysis simulations (ERA5 and MERRA2) do not capture the daytime persistence of the jet and underestimate the speed of the jet throughout the diurnal cycle. The largest absolute errors of over 4.5 m.s^{-1} (-35%) occur at 0900 LT. The reanalyses also fail to simulate the elevated subsidence inversions above the jet and associated dry layer in the lower troposphere.

1. Introduction

The Turkana Jet is a year-round feature of East African climate. The southeasterly low-level jet forms the inland branch of the large-scale offshore winds in the western Indian Ocean, which reverse from northeasterly in December-February to southwesterly in June to September. Across much of the year, the jet crosses hemispheres as it flows inland to the African interior (Figure 1). The jet core is in the Turkana Channel, between the Ethiopian and Kenya Highlands in northwest Kenya, where pilot balloon observations have recorded fast jet speeds of up to 50 m.s^{-1} (Kinuthia 1992). Jet-related low-level divergence prevents the development of a summer rainfall season in northern Kenya (Nicholson 2016), while the jet is also an important conduit for water vapour transport to the African interior (Viste and Sorteberg 2013). A stronger Turkana Jet is associated with rainfall deficits in East Africa (Munday et al. 2021; King et al. 2021; Munday et al. 2023), while moisture transport to the jet exit region contributes to higher rainfall in South Sudan (Vizy and Cook 2019). The Turkana Jet is part of the wind system which powers Africa's largest wind farm – the Lake Turkana Wind Project (Haller et al. 2022).
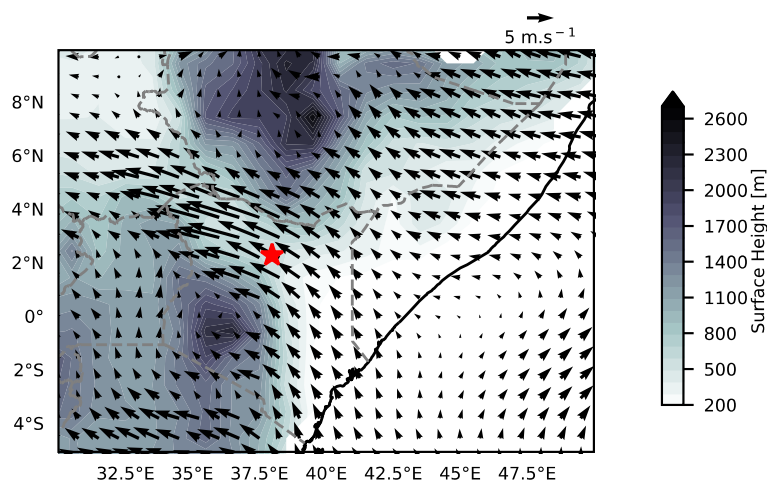

Figure 1 Turkana Jet winds at 850 hPa (vectors; m/s) during the IOP (26th March to 23rd April 2021) with surface height [m] shaded. The red star marks the position of Marsabit.

Over the last several years, our understanding of the Turkana Jet has evolved with the availability of reanalysis and model data. Nicholson (2016) provides the first full climatology of the Turkana Jet and its annual cycle in ERA-interim reanalysis. Other studies focus on; the mechanisms associated with jet maintenance and variability (Indeje et al. 2001; Hartman

3

2018; Vizy and Cook 2019; King et al. 2021; Talib et al. 2023); the role of the jet in water vapour transport (Munday et al. 2022, 2023); and its representation in models (Misiani et al. 2020; King et al. 2021; Lino et al. 2022). The recent science aimed at understanding the jet builds on two older observational studies using pilot balloons, which first quantified the jet (Kinuthia and Asnani 1982), and which documented its variability in space within the Turkana Channel (Kinuthia 1992).

With model-based understanding of the jet evolving, we need observations to provide a benchmark for models and to test mechanisms for jet maintenance and variability. The pilot balloon data from the 1980s neither provides measurements during the night, when the jet is strongest, nor measures the thermodynamics associated with jet formation. Meanwhile, there are unquantified sources of error in the pilot balloon tracking technique, which relies on the assumption of a constant rate of uplift of balloons affected by turbulence. The data shortage, and large discrepancies between pilot balloon and reanalysis data (e.g. Nicholson 2016), motivated a month-long intensive observation period (IOP): the Radiosonde Investigation for the Turkana Jet (RIFTJet; Munday et al. 2022).

RIFTJet measurements took place from 26th March to 23rd April 2021 in Marsabit, northwest Kenya (Figure 1), which is at the jet entrance region in reanalysis data. Kinuthia and Asnani (1982) first identified the Turkana Jet at Marsabit in pilot balloon data (Kinuthia and Asnani 1982), and Kinuthia (1992) notes that the jet is stronger at Marsabit compared to other sites within the Turkana Channel. March-April is the normal time of rainfall onset in the Turkana Channel. The dataset comprises eight-times daily soundings (209 total) to observe the diurnal cycle of atmospheric winds, temperature, and water vapour. In this paper, we aim to:

1. Document the observed characteristics and diurnal cycle of the Turkana Jet
2. Investigate the relationships between the jet and inversions
3. Assess the simulation of the jet and associated thermodynamic environment in two modern reanalyses.

2. Background

Figure 2 shows an example a radiosonde wind profile from Marsabit on 8th April 2021, 0000 LT. The presence of a low-level jet (LLJ) is clear, with low-level wind speed maximum of 15

4

m.s^{-1} and a vertical speed shear of ~14 m.s^{-1} in the 700 m above the jet core. The fast jet winds can be understood to first order as a consequence of channeling of large-scale flow through the Turkana Channel, between the Kenya and Ethiopian Highlands (i.e. a gap wind; Figure 1) (Indeje et al., 2001, Munday et al., 2023). Munday et al. (2022) employed a simple jet detection method stipulating jet presence based on wind speed change with height (shear) of >4 m.s^{-1} in the 800m above the jet maximum, and a maximum wind speed of at least 8 m.s^{-1} in the first kilometer above the surface. This method is tailored to the radiosonde observations providing a more conservative detection method compared to the commonly used Bonner criterion (Bonner 1968) which allows the shear to be calculated over 2 km above the jet peak. Restricting the detection to the first kilometer above the surface is important in the Turkana case since there is often a secondary, northeasterly jet, which forms higher than 2 km above the surface (Gatebe et al. 1999; Dyer and Washington 2021; Munday et al. 2022) We use the same approach to detect low-level jets in the present paper.
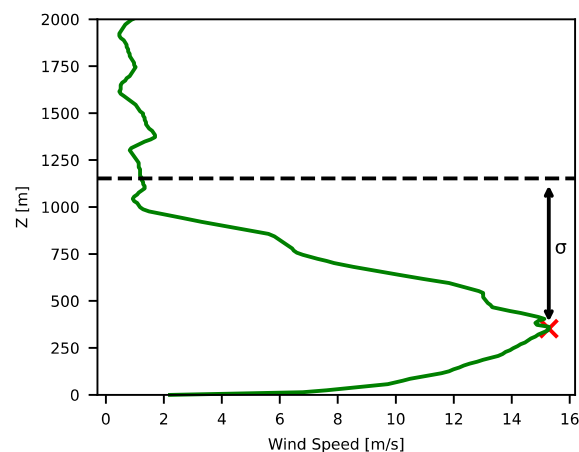

Figure 2 Radiosonde wind speed profile (m/s) from 8th April 2021, 00:00 LT. σ indicates wind speed shear above the jet core, the dotted line marks 800 m above the jet core, the red cross marks the LLJ maximum.

Based on this detection scheme, Munday et al. (2022) show that the Turkana Jet was present on 75% of soundings (out of a total of 209), with a peak in detection during the night at 0300 LT (93% of soundings). Kinuthia and Asnani (1982) first hypothesised the nocturnal peak in jet strength, but Nicholson (2016) was the first to document the 0300 LT wind maximum in reanalysis data. While the daytime jet is barely discernible in reanalysis data (e.g. Nicholson 2016, Vizy and Cook 2019, Munday et al., 2022), observations demonstrate that a low-level

5

jet often persists through the day (Kinuthia and Asnani 1982, Kinuthia 1992, Munday et al., 2022).

The mechanisms controlling the diurnal cycle of the Turkana Jet have received little attention. Hartman (2018) and Vizy and Cook (2019) argue that the nocturnal strengthening in wind speeds is driven by changes in horizontal baroclinicity due to a steepening thermal gradient between jet entrance and exit regions at night. Hartmann (2018) also suggests that overturning circulations in reanalysis, initiated by the land breeze from Lake Victoria, enhance subsidence in the Turkana Channel during the day. Hartman (2018) argues that the enhanced subsidence could lead to further daytime warming which could disrupt the jet circulation. Alternatively, the subsidence might be a mechanism for the maintenance of elevated inversions close to the low-level jet top height identified in Munday et al. (2022). More generally, surface heating-induced eddy viscosity during the day introduces boundary layer friction, which slows down jet circulations (Blackadar 1957). The development of a nocturnal stable boundary layer removes the frictional constraint, resulting in faster winds. Since reanalyses are unable to simulate the persistence of the jet through the day, it has not been possible to assess the mechanisms controlling the daytime jet.

Other mechanisms invoked to explain fast low-level jets elsewhere in the world include the role of elevated subsidence inversions. Fast low-level jets (> 30 m.s^{-1}) in the tropics are observed over isolated islands beneath the trade wind inversion. Desouza et al. (1971) reports a daytime low-level jet reaching peak speeds of 40 m.s^{-1} over Barbados (13°N, 59°W). The fast winds there are associated with a Venturi effect, whereby ambient trade winds (4-6 m.s^{-1}) are vertically constrained by the higher island topography and a subsidence (trade wind) inversion at lower atmospheric levels. Meanwhile, instances of fast gap winds in the Gibraltar strait ("the Levanter", 36°N,6°W) occur as subsidence inversions, ~1000 m above the surface, suppress the upward mixing of momentum (Capon 2006).

In the Arabian Sea, northeast of the East African landmass, data from dropsonde observations during MONEX 1979 show that the monsoonal boundary layer features an elevated capping inversion between 900-700 hPa at a similar height to a low-level wind speed maximum (Holt and Sethuraman 1985). The RIFTJet radiosonde data reveal persistent elevated inversions at ~800hPa (~500 m above the surface), close to the level of the jet, with inversion strengths of

6

between 1-3°C (Munday et al., 2022). These inversions could play a role in jet characteristics and the jet diurnal cycle.

The paper proceeds first by characterizing the Turkana Jet, and its full diurnal cycle, in the RIFTJet radiosonde data. We then investigate the relationship between the inversions and jet dynamics, with a focus on the diurnal cycle. We conclude the analysis by considering how the jet diurnal cycle and the associated thermodynamics are represented in reanalysis data.

3. Data

Data are from the RIFTJet field campaign (Munday et al., 2022), which took place from March 26th to April 23rd 2021 in Marsabit, NW Kenya. Radiosondes were released every three hours from the Marsabit WMO station, at 0000 LT through to 2100 LT, giving a sample of 209 regular releases. Additional releases outside of Marsabit and higher frequency releases are not considered here. Measurements, from GRAW DFM-09 and DFM-17 radiosondes, include pressure, temperature, humidity and winds (derived from GPS). Two automatic weather stations at 2 m and 10 m provide measurements of wind, temperature, rainfall, pressure and humidity at 1 minute resolution.

We test two modern reanalyses against the radiosonde data: the European Centre for Medium-range Weather Forecasting (ECMWF) ERA5 reanalysis (Hersbach et al. 2020) and NASA's MERRA2 reanalysis (Gelaro et al. 2017). Both reanalyses are used extensively in an African climate research context and have been used to characterise the attributes and drivers of the Turkana Jet (Vizy and Cook 2019; Hartman 2018; King et al. 2021). At the equator, MERRA2 grid size is approximately 55 km x 70 km (0.5° latitude x 0.625° longitude), and ERA5 of ~ 30 km x 30 km (0.25° latitude x 0.25° longitude). The vertical resolution in the two reanalyses is similar in the lower troposphere: between 1000 and 500 hPa, ERA5 has 16 vertical levels and MERRA2 has 17 vertical levels. Where upper-air radiosonde observations are sparse (there are only three reporting stations in East Africa), reanalysis data becomes reliant on their model physics and assimilation schemes. The radiosonde observations offer an out of sample test of the reanalysis simulations. We compare three-hourly radiosonde records with three-hourly reanalysis data at the nearest grid point to the sonde releases. We note that there are some uncertainties associated with comparing gridded data with a single

7

point, but it is a necessary procedure, including for evaluating LLJs (e.g. Laroche and Sarrazin 2013; Berg et al. 2015)

An overview of the synoptic conditions during the IOP are given in Munday et al. (2022). March to April is the normal time of rainfall onset over NW Kenya (Dyer and Washington 2021), but in 2021 rainfall onset was delayed, with rainfall deficits of 70 mm. The poor rains over the whole March-May ("long rains") season are part of a multi-year drought across East Africa. The data, therefore, are representative of the period prior to full rainfall onset in generally dry conditions. The connection between the Turkana Jet and remote drivers, including ENSO, are not well established, however, it is worth noting here that 2021 featured a weak La Nina event which could have influenced jet characteristics.

4. Low-level jet characteristics

This section documents the distribution of LLJ characteristics during RIFTJET. Figure 3 presents histograms for the LLJ wind speed maximum, wind speed shear, height, and direction. Note that the focus in this section is on the 158 radiosonde releases (out of 209 three-hourly sondes) for which low-level jets were detected. Twenty-eight percent of jets reach maximum speeds of between 14 and 16 m.s^{-1}. The jet speeds are approximately normally distributed. Five percent of jets maximum speeds were between 8-10 m.s^{-1} (8 m.s^{-1} is the minimum according to the jet detection method) and 6% of jet speed maxima were above 20 m.s^{-1}. The mean jet speed of 15.0 m.s^{-1}, is similar or higher in comparison to other observed African LLJs in the Sahara (Allen and Washington 2014; Washington et al. 2006) and Namibia(Clements and Washington 2021)

The distribution of jet-related vertical wind shear - calculated as the difference between the jet maximum and the minimum wind speed in the 800m above the jet - is positively skewed. The mean shear for jet cases is 8.9 m.s^{-1} over 800 m, which corresponds to 1.1 m.s^{-1}/100 m. In a few cases, the low-level shear exceeded 16 m.s^{-1} - although in ~45% of jet cases the shear was below 8 m.s^{-1}. The strong vertical wind shear is likely to inhibit the transition from shallow to deep convection as mechanical mixing between the cloud and its environment dilutes the cloud core (Markowski and Richardson 2010).

LLJs formed close to the surface in most cases (Figure 3c). The height of the maximum jet wind speed is most commonly between 300-400 m above the surface (37% of LLJs).

8

There were six instances when the jet formed < 200 m above the surface, and only two occasions when the jet height was greater 800 m. The jet direction (Figure 3d) is most commonly southeasterly (120-140°), corresponding to the orientation of the Turkana Channel. Around 12% of jets have a larger easterly component with directions between 90 and 110°.
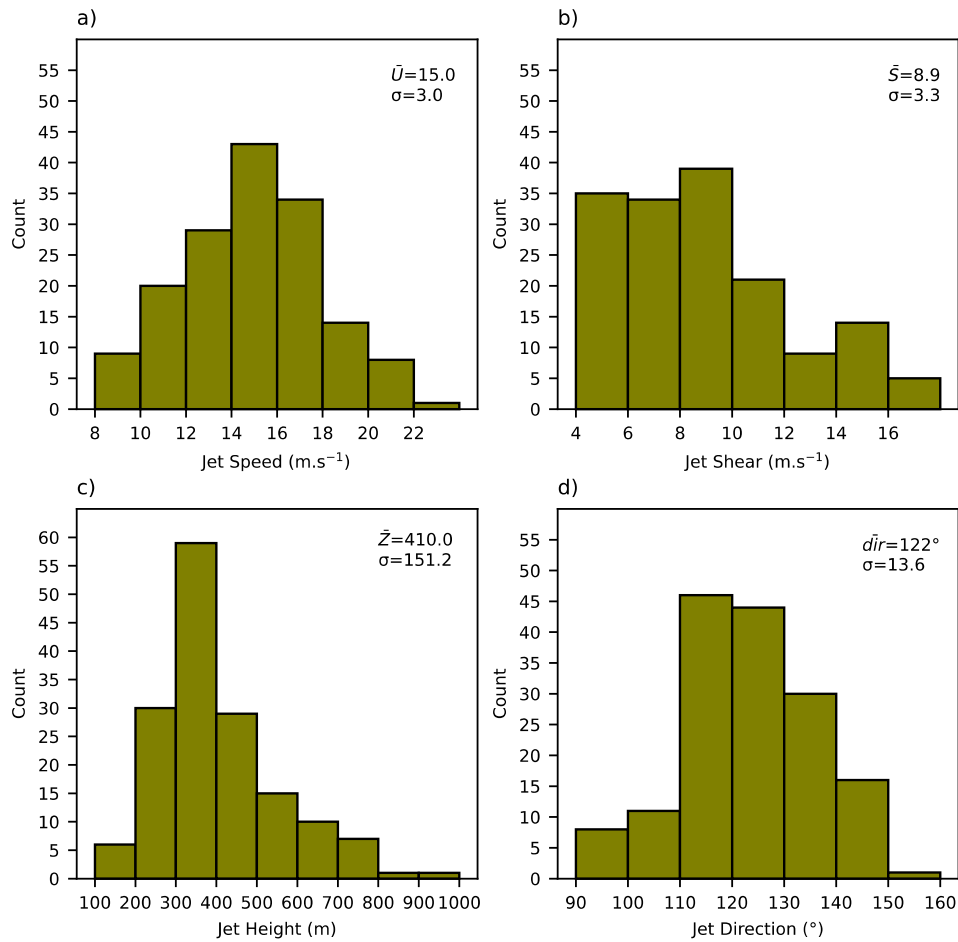

Figure 3 Distribution of characteristics for 158 detected LLJs. Wind speed [m/s] (a), shear in 800 m above jet core [m/s] (b), height of jet maximum [m] (c), jet direction [°] (d). Text in upper right of figures shows mean values and standard deviations.

9

5. Diurnal cycle of lower-level winds

This section presents the diurnal variation in lower-tropospheric wind speeds (Figure 4). We investigate the full sample of 209 3-hourly soundings, to ensure that the sample sizes for each time of day are comparable (since jets are more frequent during the night). There is significant diurnal variability in wind speeds in the 4500 m above the surface. We first consider the diurnal variability associated with the low-level jet (the Turkana Jet), which is found within 1000 m of the surface (Section 4).
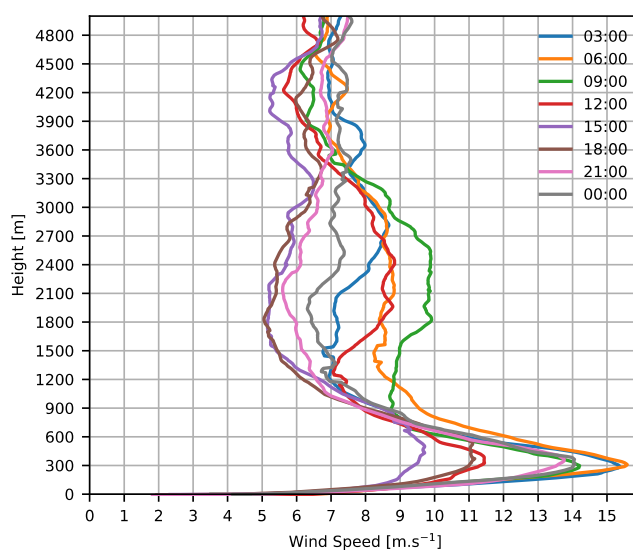

Figure 4 Wind speed (m/s) profiles by height (m) in lower-troposphere for 3-hourly radiosondes (local time)

The average wind speed profile for all times of day features a clear LLJ structure, with a maximum below 600 m, and vertical wind speed shear maintained through the 1000 m layer above the jet maximum (Figure 4). The maximum low-level wind speed (<1000 m a.s.l) is strongest at 0300 LT (16.8 m.s^{-1}, s.d=2.6 , n=27) and 0600 LT (16.5 m.s^{-1}, s.d = 2.6, n=23), and weakens during the day to the minimum at 1500 LT (10.9 m.s^{-1}, s.d = 2.6 , n=27) (Table 1). For the soundings between 2100 LT and 0900 LT, the average wind speed maximum is >14 m.s^{-1}. This is consistent with the diurnal cycle in jet detection (Munday et al., 2022), with the peak jet detection at 0300 LT (93% of days), and minimum jet detection at 1500 LT (52% of days).

10

Table 1 Lower-level wind characteristics by time of day, for winds below 1000 m above surface. Number of radiosondes is given next to times of day. Bold text indicates mean values, normal text is standard deviation.

Time (EAT)	Wind speed maximum (m.s⁻¹)		Height of wind maximum (m)		Direction of Wind maximum (°)	
15:00 (n=27)	**10.9**	2.6	**528**	239	**115**	11.1
18:00 (n=27)	**12.2**	2.5	**528**	189	**112**	16.0
21:00 (n=27)	**14.4**	2.8	**388**	97	**120**	14.6
00:00 (n=27)	**15.2**	2.9	**353**	125	**126**	23.5
03:00 (n=27)	**16.8**	2.6	**350**	104	**132**	9.6
06:00 (n=23)	**16.5**	2.6	**378**	129	**135**	13.8
09:00 (n=25)	**15.5**	2.8	**342**	128	**134**	13.9
12:00 (n=26)	**12.4**	2.8	**460**	202	**126**	20.2

The height of the wind maximum varies through the diurnal cycle, with a preference for LLJs to form higher above the surface during the day, and lower during the night and early morning. For example, the average height of the low-level wind maximum at 1500 LT is 528 m (s.d =239, n=27), while it is 342 m (s.d = 128 m, n=25) at 0900 LT. The pilot balloon data from Marsabit in March and April 1980 report a jet core that is higher (610 m) at 0900 LT. At 1500 LT, the height of the jet in the pilot balloon data is 305 m in March 1980 and 610 m in April 1980 - with the radiosonde data similar to the latter. The measurement interval in the pilot balloon data is every 152 m, compared to ~10 m in the radiosonde data (in the first 1 km above surface). The differences between pilot balloon and radiosonde data could result from interannual variability, the documentation of which requires longer-term monitoring of the Turkana Jet through multiple years.

The LLJ tends to be east-southeasterly during the day, turning southeasterly at night and early morning (Figure 5). There is significant directional shear above the jet. Between 2100 LT and 1200LT the winds turn anticyclonically with height through ~90° from southeasterly below 1000 m to northeasterly between ~1200 and 3000 m (Figure 5). At 1500 LT and 1800 LT, the directional shear reduces, with east-south-easterlies (95-120°) through the lower troposphere.
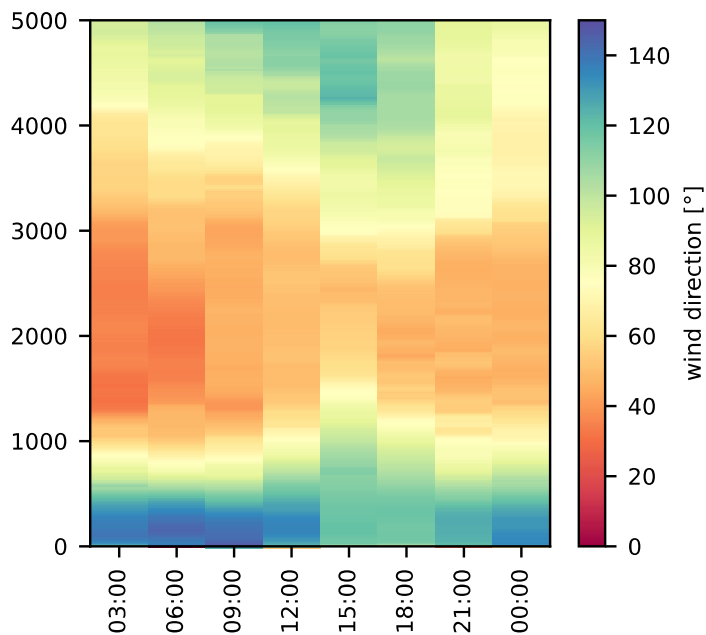
11

Figure 5 Diurnal cycle in wind direction (°) by height for 3-hourly radiosonde data (local time)

There is a large diurnal range in wind speeds associated with the northeasterlies above ~1200 m (Figure 4). The northeasterlies tend to be strongest during the morning form 0600 LT to 1200 LT (>10 m.s^{-1}), reaching a maximum speed at 0900 LT. The northeasterlies are weaker during the afternoon and early evening (<7 m.s^{-1}). Between 1200 LT and 1500LT, the northeasterly layer weakens and reduces in vertical extent. The northeasterlies were identified by Kinuthia (1992) and others (e.g. Gatebe et al. 1999; Dyer and Washington 2021) but, to the authors knowledge, the diurnal cycle in these winds has not previously been shown. It is beyond the scope of the study to investigate the causes of this variability. One hypothesis is that it relates to the cycle of heating and cooling over the Ethiopian Highlands to the northeast of the Turkana Channel.

The diurnal cycle of mean winds close to the surface, at 2 m and 10 m, is distinct from the diurnal cycle of the low-level jet (Figure 6). At 2 m, average winds peak at 0730 LT (4.2 m.s^{-1}) - roughly an hour after sunrise - likely as momentum from the jet is mixed down to the surface with the onset of surface heating. The minimum (2.2 m.s^{-1}) is at 1800 LT, when a weak surface-based inversion between 2 m and 10 m starts to form due to radiative cooling (Munday et al., 2022). Ten-meter winds are faster than at 2 m throughout the diurnal cycle, with a higher degree of variability. Winds at 10 m are fastest through the early morning hours

12

from 0200 LT, increasing in speed up 6.5 m.s^{-1} at 1030 LT. There is some indication of separate 10 m wind maxima at 0230 LT and 0645 LT. After the morning peak, 10 m wind speeds drop off towards the minimum just after 1800 LT (4.3 m.s^{-1}) .
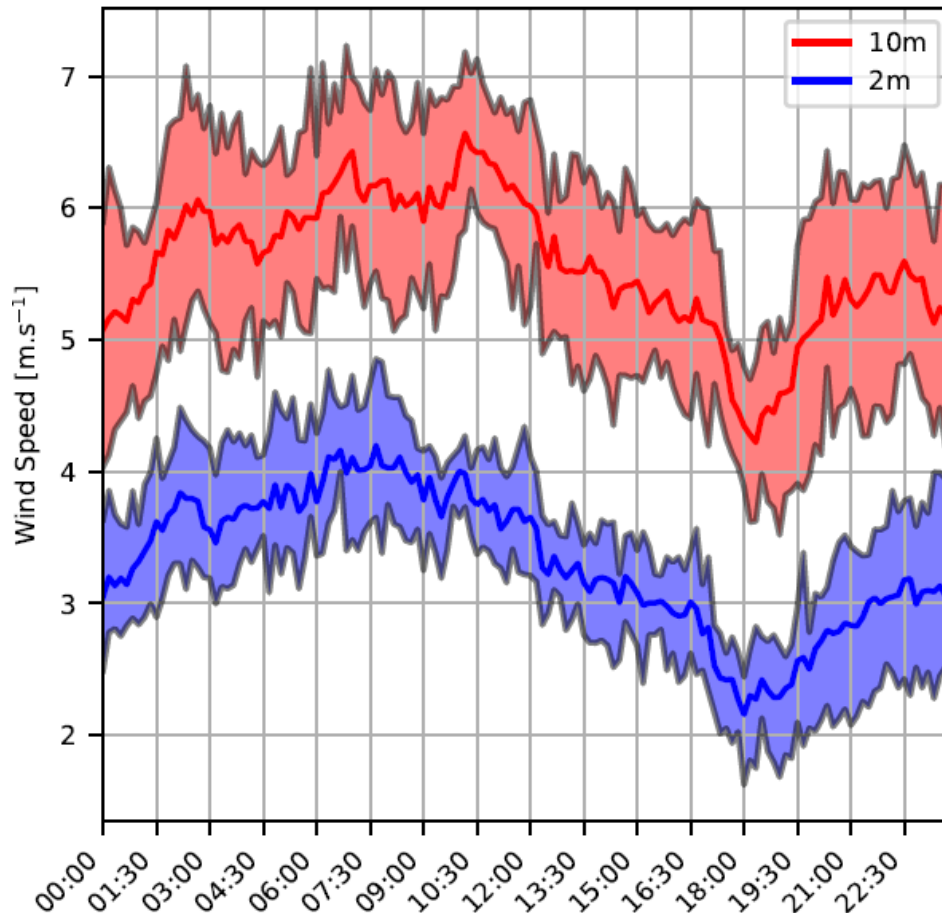

Figure 6 Diurnal cycle in mean wind speeds at 10 m (red) and 2 m (blue) from 10-minute averaged AWS data. The filled contours represent the 25th and 75th percentile values.

6. Inversions and the low-level jet

The relationship between surface-based inversions and nocturnal low-level jets has been demonstrated in a variety of contexts (Blackadar 1957; van de Wiel et al. 2010; Yabra et al. 2022). The development of a surface-based inversion decouples surface friction from the overlying atmosphere, which can lead to an acceleration of winds. The Turkana Jet is,

13

however, an interesting case. The jet can occur through the day, when radiative surface-based inversions are generally absent, and the most persistent temperature inversions form above the surface at a height of between 200 and 800 m (Munday et al., 2022). This section analyses the relationship between inversions and the jet.

We first consider surface-based inversions (Figure 7), defined as an inversion with a base within 20 m of ground level. Apart from one very weak inversion (<0.1°C) at 1200 LT, surface-based inversions form preferentially in the evening and through the night. The surface inversions are weak (<0.5 °C), and reach a maximum frequency at local midnight, occurring on 42% 0000 LT soundings. The frequency of surface-based inversions is much lower than the frequency of jet formation throughout the diurnal cycle. For example, at 0900 LT, a LLJ is present on 78% of soundings, but there are no instances of surface-based inversions. The development of surface-based inversions is therefore not a necessary condition for the formation of the Turkana Jet.
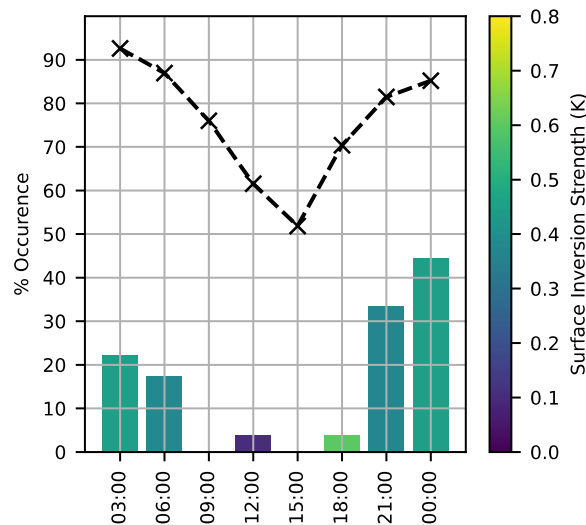

Figure 7 Percent of radiosonde profiles with surface-based inversions for each 3-hourly release time (bars) and their mean strength (shading). Surface based inversions are defined as temperature inversions starting within 20 m of the surface. The black dashed line shows the % of radiosonde profiles when a LLJ is detected for each 3-hourly release time (defined in Section 2).

Next, we consider the elevated inversions which form closest to the jet but above the land surface. Munday et al., (2022; their Figure 10) shows that these elevated inversions are a persistent feature through the campaign. Figure 8 shows the average diurnal cycle in the height of the mid-point of the elevated inversions along with the height of the jet maximum.

14

During the night, the inversions form on average 380 m above the land surface, rising to 650 m at 1500 LT with daytime surface heating. The height of low-level jets follows a similar pattern: the average height of daytime jets is below 600 m, while they form closer to the surface (~350 m) and strengthen during the night. The jets mainly form below the inversion throughout the diurnal cycle. The elevated inversions are strongest in the early morning hours (>1°C) and weakest in the later afternoon (0.5-0.8°C), inversely correlated with the inversion height and the strength of the jet. A stronger, and lower inversion tends to be associated with a faster jet. Establishing cause and effect in this context is difficult. For example, the jet-related divergence, which is not possible to assess from a single site, could feedback on the strength of the inversion through enhanced subsidence.
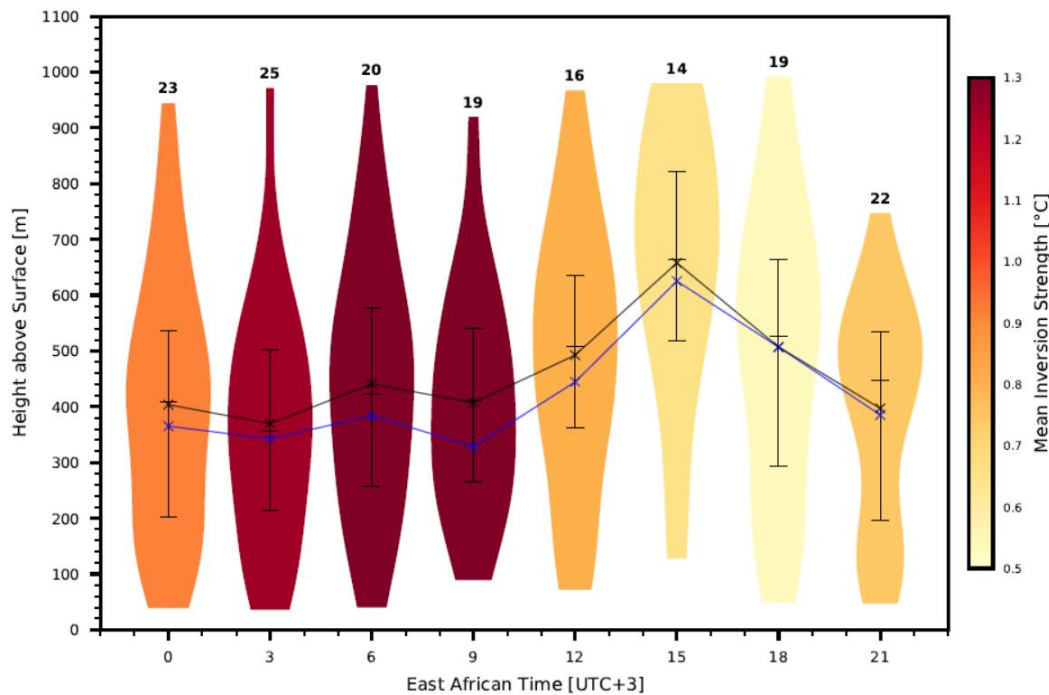

Figure 8 Diurnal cycle of inversions and the LLJ. Violin plots indicate the height distribution [m] of the inversion mid-points, with the shading indicating the average inversion strength [°C]. The black line is the mean altitude of the inversions, with the median and interquartile range indicated by the bars. The blue line shows the diurnal cycle in mean jet altitude. The value above the violins is the number of jet cases for that time of day. The plot does not include surface-based inversions.

Figure 9 shows an example of the diurnal evolution of winds and lower-atmospheric temperature structures for the night with the strongest recorded jet of 23.4 m.s^{-1} on the 10th –

15

11th April 2021. The inversion (at 840 hPa, 1575 m) starts to form at 2100 LT and strengthens through to 0300 LT, along with the increase in wind speeds to their maximum at 0300 LT. At 0600 LT the height of the inversion rises, in tandem with increased height and weakening of the LLJ. At 0900 LT, the inversion height drops down to 850 hPa with the jet maximum height also lowering to this level and strengthening again. By 1200 LT the inversion dissipates, and the wind maximum height rises again to 820 hPa. This case study is indicative of the close coupling between the inversions and jet dynamics.
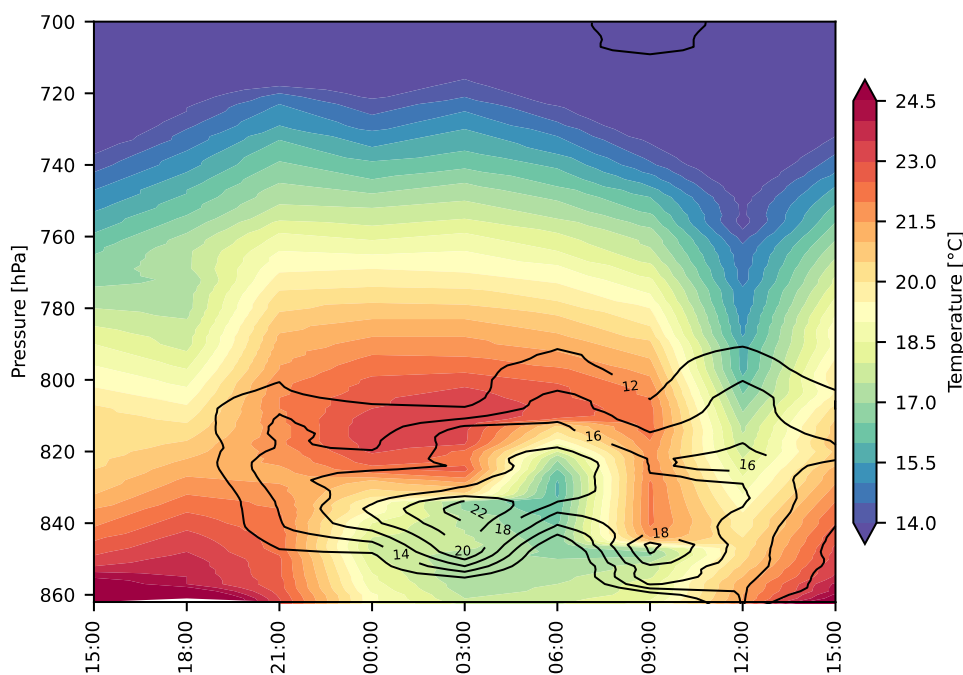

Figure 9 Diurnal evolution of temperature (shading) and wind speed above 12 m.s^{-1} (contours) from 1500 LT on 10th April to 1500 LT on 11th April. Contour interval is 2 m.s^{-1}.

7. Diurnal cycle errors in reanalysis

Given the scarcity of upper air observations in East Africa, the RIFTJet data offer a unique opportunity to evaluate the performance of modern reanalysis products in the region. Qualitative analysis suggests that ERA-Interim underestimates the speed of the jet, compared to PiBAL data (Nicholson 2016), while Munday et al. (2022) report ERA5 underestimation

16

of the jet maximum speed at both 0300 LT and 1500 LT. Here, we investigate the representation of the full diurnal cycle of the lower atmosphere for the RIFTJET period in two modern reanalyses: MERRA2 and ERA5.

Figure 10 shows large differences in the average wind speed profile for different times of day between MERRA2 and ERA5. In MERRA2, the jet forms at 900 hPa, while in ERA5 the height of the maximum wind speed is at 850 hPa. Both reanalyses simulate the nocturnal acceleration of winds and capture the peak winds at 0300 LT and 0600 LT shown in the radiosonde data (Figure 4). A clear bias in the reanalyses is the lack of daytime persistence of the clear low-level jet structure seen in radiosonde data (Figure 4). In MERRA2, winds are approximately constant with height through the lower atmosphere up to ~775 hPa at 1200 LT, 1500 LT and 1800 LT. ERA5 is marginally better, producing a subtle peak in wind speeds at the approximate height of the nocturnal jet, but with very little shear. Above the LLJ, the reanalyses also underestimate the amplitude of the diurnal cycle of northeasterly flow between 750 and 650 hPa, which is 5 m.s^{-1} in radiosonde data (Figure 4) but 2.1 m.s^{-1} in ERA5 and 3.5 m.s^{-1} in MERRA2. Both reanalyses simulate peak winds associated with the northeasterlies at 0600 LT rather than 0900 LT as is recorded in radiosonde data (Figure 4).
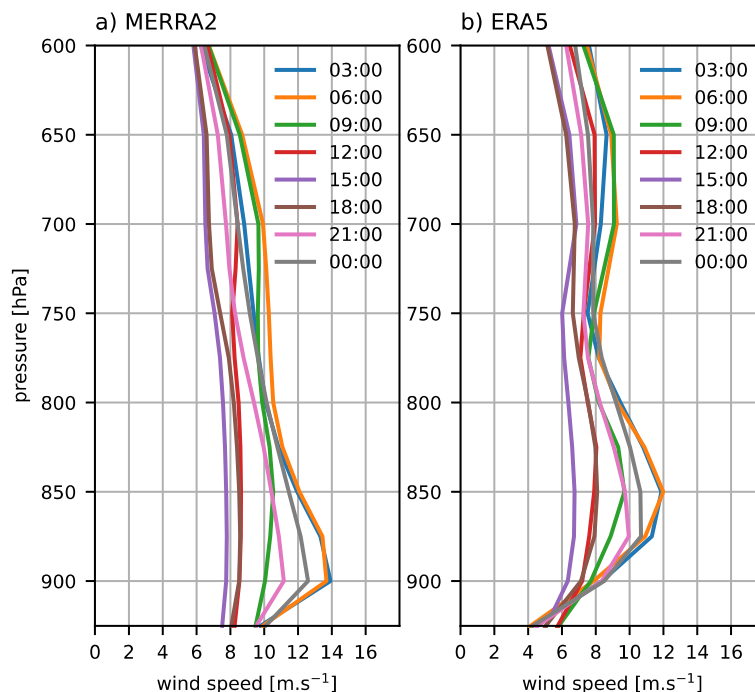

Figure 10 Wind speed (m.s^{-1}) profiles by pressure (hPa) in lower-troposphere for 3-hourly MERRA2 (a) and ERA5 (b).

17

Figure 11 confirms the underestimation of Turkana Jet windspeed throughout the diurnal cycle during the IOP. Large absolute errors occur at 0300 LT when the maximum wind speed is underestimated by 4.4 m.s^{-1} (-26 %) in ERA5. MERRA2 performs better in simulating the higher wind speeds during the night, although still underestimates the wind maximum by 2 m.s^{-1}. Between 0600 LT and 0900 LT, maximum wind speeds decrease sharply to ~11 m.s^{-1} in reanalysis but remains high (~15.5 m.s^{-1}) in reality, an error of -35%. In the radiosonde data, the steepest decline in morning wind speeds occurs between 0900 LT and 1200 LT. The minimum at 1500 LT is captured by both ERA5 and MERRA2, but the wind speed is ~3 m.s^{-1} lower than the radiosonde observations. While the focus here is on the average diurnal cycle, we note that for individual soundings, the difference between reanalysis and radiosonde low-level wind maximum can exceed 6 m.s^{-1} (not shown).
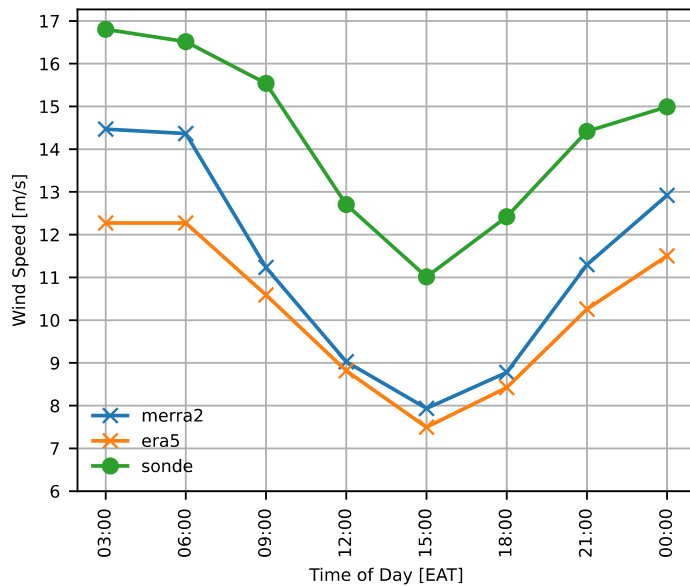

Figure 11 Diurnal cycle of low-level (>700 hPa) mean maximum wind speeds in radiosonde (green), MERRA2 (blue) and ERA5 (orange)

Errors in the reanalysis winds are accompanied by errors in their representation of the temperature structure of the lower atmosphere. Figure 12 shows three key differences between radiosonde and reanalysis in the mean diurnal cycle of lower-tropospheric temperature and winds (above 10 m.s^{-1}). First, the wind maximum is too broad in reanalysis:

18

windspeeds above 10 m.s^{-1} in sonde data are constrained to a 50 hPa layer between 850 hPa and 800 hPa, whereas in MERRA2 winds above 10 m.s^{-1} occur in a 150 hPa layer from ~900 hPa to ~750 hPa. Second, the heating profiles in the boundary layer are far too strong during the day in both reanalysis datasets, which is caused in part by topographic related errors in surface pressure (Munday et al., 2022) - the surface height at the release site is underestimated in both ERA5 (799 m) and MERRA2 (624 m), compared to reality (1337 m). Third, neither reanalysis captures the non-surface inversion layer above the jet at ~800 hPa which is present in the radiosonde data through the night and morning from 0300 LT to around 1000 LT. The inversion layer in radiosonde is between 19.5 and 21°C at 825-800 hPa, whereas the temperature is between 18 and 16°C at this height in both reanalyses, with no evidence of an inversion. Since the inversions prevent the upward mixing of momentum, this is a possible explanation for the generally slower wind speeds and lack of daytime persistence of the jet in reanalysis.
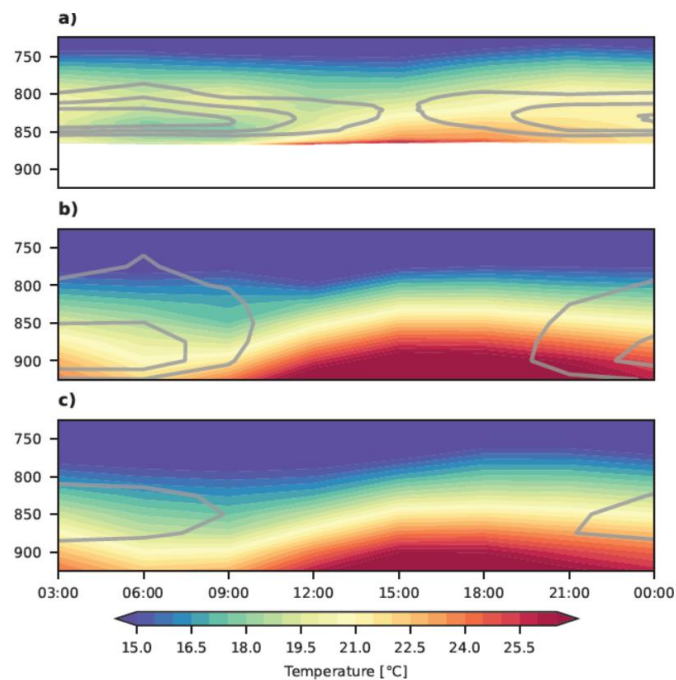

Figure 12 Diurnal cycle of lower-tropospheric temperature (°C; shading) and winds above 10 m.s^{-1} (grey contours at 2 m.s^{-1} intervals) in a) radiosonde, b) MERRA2 and c) ERA5

19

In radiosonde data, subsidence associated with the elevated inversions leads to drying in the 500 -1000 m above the jet maximum (Figure 13). The dry layer is strongest during the night and early morning (relative humidity 40 - 50 %) when the elevated inversions are strongest. During the afternoon from 1200 LT to 1500 LT moist near-surface air is mixed upwards as the inversions weaken. The drying in the layer above the jet resumes in the evening from 1800 LT onward, with the redevelopment of the strongest elevated inversions. A second layer of higher humidity air is associated with the northeasterly flow between 725 and 625 hPa (2000 m a.s.l), and develops from 0000 LT through to 1200 LT.

In reanalysis, these features are poorly simulated (Figure 13). The dry layer between 825 hPa and 725 hPa is not present, and so neither is its diurnal cycle. While there is evidence of upward mixing of surface moist air in the day, the relative humidity is too high (above 90%) at 1500 LT in the layer between 825 and 725 hPa – where it is ~70% in radiosonde data. There is also a low bias in relative humidity close to the surface in both reanalysis during the day, related to the excessive boundary layer heating. More reassuringly, the reanalyses do simulate the drier air above 650 hPa.
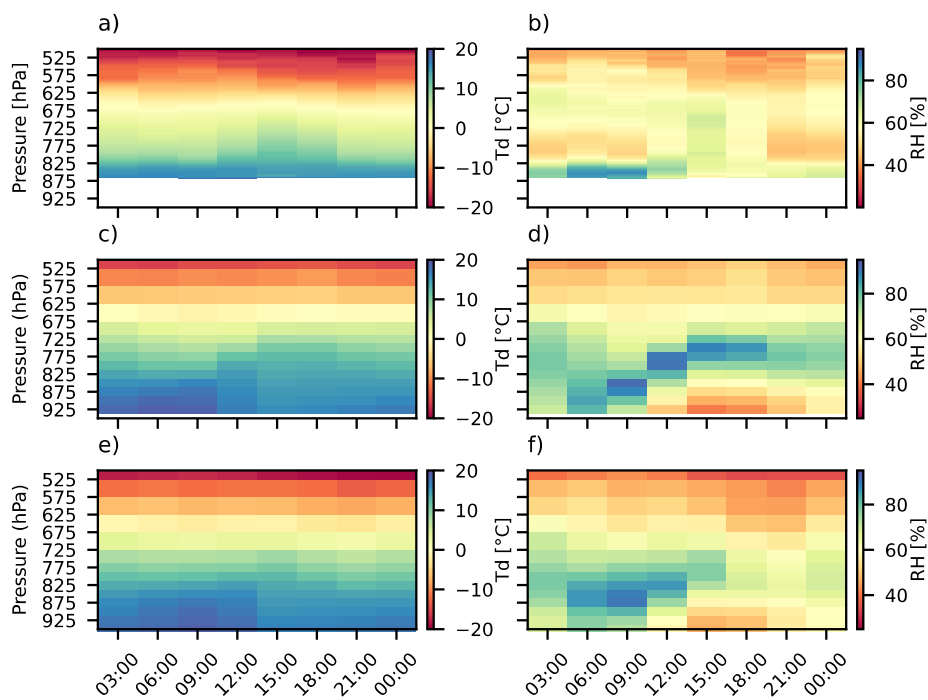

Figure 13 Diurnal cycle of lower-tropospheric dewpoint temperatures (°C; first column) and relative humidity (%; second column) First row (a-b) is radiosonde data, second row (c-d) is MERRA2 and third row is ERA5 (e,f)

20

8. Conclusion

This paper describes the observed characteristics and diurnal cycle of the Turkana Jet. The southeasterly jet forms close to the surface ($\bar{Z}$=410 m) with high average maximum wind speeds of 15.0 m.s^{-1}. There is substantial shear above the jet core (8.9 m.s^{-1} over 800 m). The jet has a clear diurnal cycle, with the strongest low-level winds detected during the night (16.8 m.s^{-1}, 0300 LT) and weakest during the day (10.9 m.s^{-1} at 1500 LT). A key finding is the tendency of fast jets of over 12 m.s^{-1} to occur throughout the day, particularly in the morning hours up to 1200 LT.

The diurnal cycle of the Turkana Jet is closely related to the diurnal cycle in elevated inversions, shown schematically in Figure 14. These inversions are strongest and lower to the ground during the night, with the mid-point of the inversion tending to form 20-60 m above the LLJ. The stable layer inhibits the upward mixing of momentum and could contribute to the nocturnal strengthening of the jet. The daytime weakening and lifting of the elevated inversion likely operates in tandem with the weakening of the large-scale horizontal temperature gradients during the day (Vizy and Cook 2019; Hartman 2018), and the increase in eddy viscosity to produce the observed jet diurnal cycle. During the mid-afternoon, the height gradient between jet entrance and exit regions is low (<3 m across ~ 600 km in reanalysis; Vizy and Cook 2019) and eddy viscosity is high, leading us to hypothesise that the elevated subsidence inversions play a role in the daytime persistence of the jet (on over 50% of days). Testing this hypothesis relies on idealised experiments with models that can capture the inversions.

Modern reanalyses simulate winds that are weak compared to the radiosonde data and do not capture the daytime persistence of the jet. The errors maximise at 4.5 m.s^{-1} (-35%) in ERA5 at 0900 LT, with MERRA2 performing marginally better. The higher wind speeds in MERRA2 are consistent with other analyses of the Turkana Jet (Vizy and Cook 2019; King et al. 2021). One possible cause of the large errors is the limited vertical resolution, which ensures that the inversions important for maintaining jet strength and the daytime persistence of the jet are not captured. Indeed, Figure 12 shows the elevated subsidence inversions, which form on every night in the radiosonde data, are not present in the reanalysis data. The lack of subsidence inversions is associated with failure to capture a layer of dry air above the jet core present through the night in radiosonde observations. A next step, which we are taking in a

forthcoming paper, is to investigate what model resolutions are required to improve the simulation of elevated inversions and jet speed.
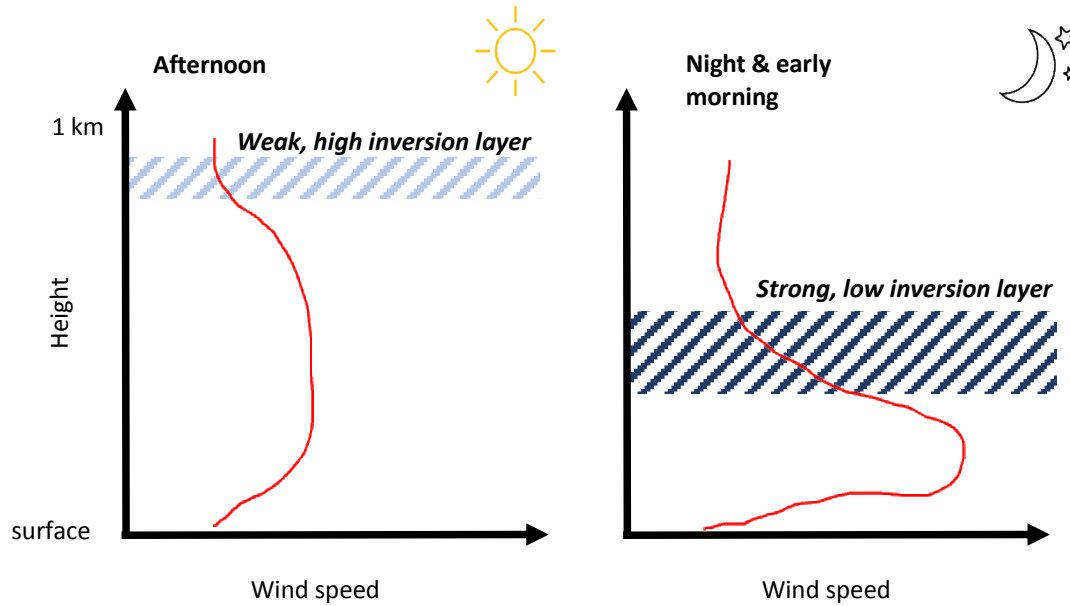

Figure 14 Schematic illustrating relationship between LLJ diurnal cycle and elevated subsidence inversions.

Data Availability Statement

MERRA2 data are from http://gmao.gsfc.nasa.gov/products/ and ERA5 data are downloaded from https://cds.climate.copernicus.eu/cdsapp#!/home. USGS GTOPO30 global digital elevation model data are from http://earthexplorer.usgs.gov/. Radiosonde and AWS data from RIFTJET is available on request from the author.

REFERENCES

Allen, C. J. T., and R. Washington, 2014: The low-level jet dust emission mechanism in the central Sahara: Observations from Bordj-Badji Mokhtar during the June 2011 Fennec Intensive Observation Period. *Journal of Geophysical Research Atmospheres*, 238, https://doi.org/10.1038/175238c0.

Berg, L. K., L. D. Riihimaki, Y. Qian, H. Yan, and M. Huang, 2015: The low-level jet over the southern great plains determined from observations and reanalyses and its impact on moisture transport. *J Clim*, **28**, 6682–6706, https://doi.org/10.1175/JCLI-D-14-00719.1.

Blackadar, A. K., 1957: Boundary Layer Wind Maxima and Their Significance for the Growth of Nocturnal Inversions. *Bull. Amer. Meteor. Soc.*, **38**, 283–290.

Bonner, W., 1968: Climatology of the Low Level Jet. *Mon Weather Rev*, **96**, 833–850, https://doi.org/10.1175/1520-0493(1968)096<0833:cotllj>2.0.co;2.

Capon, R. A., 2006: High resolution studies of the Gibraltar Levanter validated using sun-glint anemometry. *Meteorol. Appl.*, **13**, 257–265.

Clements, M., and R. Washington, 2021: Atmospheric Controls on Mineral Dust Emission From the Etosha Pan, Namibia Observations From the CLARIFY‐ 2016 Field Campaign. *JGR Atmospheres*, **126**.

Desouza, R. L., M. Garstang, N. E. Laseur, and Y. Hsueh, 1971: A Low-level Jet in the Tropics. *Mon Weather Rev*, **99**, 559–563.

Dyer, E., and R. Washington, 2021: Kenyan long rains: A subseasonal approach to process-based diagnostics. *J Clim*, **34**, 3311–3326, https://doi.org/10.1175/JCLI-D-19-0914.1.

Gatebe, C. K., P. D. Tyson, H. Annegran, S. Piketh, and G. Helas, 1999: A seasonal air transport climatology for Kenya. *Journal of Geophysical Research* , **104**, 14237–14244.

Gelaro, R., and Coauthors, 2017: The Modern-Era Retrospective Analysis for Research and Applications, Version 2 (MERRA-2). *J Clim*, **30**, 5419–5454, https://doi.org/10.1175/JCLI-D-16-0758.1.

Haller, T., A. Pase, J. Warner, N. Hashimshony-Yaffe, A. K. García, and M. Bertoncin, 2022: Mega-infrastructure projects in drylands. *Drylands Facing Change*, Routledge, 112–131.

Hartman, A. T., 2018: An analysis of the effects of temperatures and circulations on the strength of the low-level jet in the Turkana Channel in East Africa. *Theor Appl Climatol*, **132**, 1003–1017, https://doi.org/10.1007/s00704-017-2121-x.

Hersbach, H., and Coauthors, 2020: The ERA5 global reanalysis. *Quarterly Journal of the Royal Meteorological Society*, **146**, 1999–2049, https://doi.org/10.1002/qj.3803.

Holt, T., and S. Sethuraman, 1985: Aircraft and Ship Observations of the Mean Structure of the Marine Boundary Layer over the Arabian Sea During MONEX 79. *Boundary Layer Meteorology*, **33**, 259–282, https://doi.org/https://doi.org/10.1007/BF00052059.

Indeje, M., F. H. M. Semazzi, L. Xie, and L. J. Ogallo, 2001: Mechanistic model simulations of the East African climate using NCAR regional climate model: Influence of large-scale orography on the Turkana low-level jet. *J Clim*, **14**, 2710–2724, https://doi.org/10.1175/1520-0442(2001)014<2710:MMSOTE>2.0.CO;2.

King, J. A., S. Engelstaedter, R. Washington, and C. Munday, 2021: Variability of the Turkana Low-Level Jet in Reanalysis and Models: Implications for Rainfall. *Journal of Geophysical Research: Atmospheres*, **126**, https://doi.org/10.1029/2020JD034154.

Kinuthia, J. H., 1992: Horizontal and vertical structure of the Lake Turkana jet. *Journal of Applied Meteorology*, **31**, 1248–1274, https://doi.org/10.1175/1520-0450(1992)031<1248:HAVSOT>2.0.CO;2.

——, and G. C. Asnani, 1982: A newly found jet in north Kenya (Turkana Channel). *Mon Weather Rev*, **110**, 1722–1728, https://doi.org/10.1175/1520-0493(1982)110<1722:ANFJIN>2.0.CO;2.

Laroche, S., and R. Sarrazin, 2013: Impact of radiosonde balloon drift on numerical weather prediction and verification. *Weather Forecast*, **28**, 772–782, https://doi.org/10.1175/WAF-D-12-00114.1.

Lino, O., M. Nzau J., E. Dyer, F. Opijah, R. James, R. Washington, and T. Webb, 2022: Characteristics of the Turkana low-level jet stream and the associated rainfall in CMIP6 models. *Clim Dyn*, https://doi.org/10.1007/s00382-022-06499-4.

Markowski, P., and Y. Richardson, 2010: *Mesoscale Meteorology in Midlatitudes*. John Wiley & Sons,.

Misiani, H. O., D. L. Finney, Z. T. Segele, J. H. Marsham, A. Tadege, G. Artan, and Z. Atheru, 2020: Circulation patterns associated with current and future rainfall over Ethiopia and south Sudan from a convection-permitting model. *Atmosphere (Basel)*, **11**, https://doi.org/10.3390/atmos11121352.

Munday, C., R. Washington, and N. Hart, 2021: African Low-Level Jets and Their Importance for Water Vapor Transport and Rainfall. *Geophys Res Lett*, **48**, https://doi.org/10.1029/2020GL090999.

——, and Coauthors, 2022: Observations of the Turkana Jet and the East African Dry Tropics: The RIFTJet Field Campaign. *Bull Am Meteorol Soc*, **103**, E1828–E1842, https://doi.org/10.1175/BAMS-D-21-0214.1.

——, N. Savage, R. G. Jones, and R. Washington, 2023: Valley formation aridifies East Africa and elevates Congo Basin rainfall. *Nature*, **615**, 276–279, https://doi.org/10.1038/s41586-022-05662-5.

Nicholson, S., 2016: The Turkana low-level jet: Mean climatology and association with regional aridity. *International Journal of Climatology*, **36**, 2598–2614, https://doi.org/10.1002/joc.4515.

Talib, J., C. M. Taylor, B. L. Harris, and C. M. Wainwright, 2023: Surface-driven amplification of Madden–Julian oscillation circulation anomalies across East Africa and its influence on the Turkana jet. *Quarterly Journal of the Royal Meteorological Society*, https://doi.org/10.1002/qj.4487.

Viste, E., and A. Sorteberg, 2013: Moisture transport into the Ethiopian highlands. *International Journal of Climatology*, **33**, 249–263, https://doi.org/10.1002/joc.3409.

Vizy, E. K., and K. H. Cook, 2019: Observed relationship between the Turkana low-level jet and boreal summer convection. *Clim Dyn*, **53**, 4037–4058, https://doi.org/10.1007/s00382-019-04769-2.

Washington, R., M. C. Todd, S. Engelstaedter, S. Mbainayel, and F. Mitchell, 2006: Dust and the low-level circulation over the Bodélé Depression, Chad: Observations from BoDEx 2005. *Journal of Geophysical Research Atmospheres*, **111**, 1–15, https://doi.org/10.1029/2005JD006502.

van de Wiel, B. J. H., A. F. Moene, G. J. Steeneveld, P. Baas, F. C. Bosveld, and A. A. M. Holtslag, 2010: A conceptual view on inertial oscillations and nocturnal low-level jets. *J Atmos Sci*, **67**, 2679–2689, https://doi.org/10.1175/2010JAS3289.1.

Yabra, M. S., M. Nicolini, P. Borque, Y. G. Skabar, and P. Salio, 2022: Observational study of the South American low-level jet during the SALLJEX. *International Journal of Climatology*, **42**, 9676–9696, https://doi.org/10.1002/joc.7857.